FINITE ELEMENT MODELING FOR VIBRATION ANALYSIS OF LARGE TURBO MACHINERY

Van Thanh Ngo[1, *], Danmei Xie[2], Hoai Duc Le[1]

[1]*University of Transports and Communication, Vietnam*

[2]*School of Power and Mechanical Engineering, Wuhan University, China*

[*]Email*: ngovanthanhdc@gmail.com*

Received: 7 January 2014; Accepted for publication: 12 July 2014

ABSTRACT

Recently, finite elements method (FEM) has been used most popular for analysis of stress, vibration, heat flow and many other phenomena. With the increase in computing power, FEM is wider used for the static and dynamic analysis of rotor bearing system. In this paper, the lateral vibration of large turbo machinery is studied. The FEM model is created and the eigenvalues and eigenvectors are calculated and analyzed to find natural frequencies, critical speeds, mode shapes and unbalance responses. Then critical and mode shapes are determined. Finally, responses of unbalance force are analyzed and compared in case of isotropic bearings and anisotropic bearings.

Keywords: finite element method (FEM), lateral vibration, turbo machinery, mode shape, critical speed.

1. INTRODUCTION

Lateral rotor vibration (LRV) is radial –plane orbital motion of the rotor spin axis. LRV is an important design consideration in many types of rotating machinery, particularly turbo -electrical machines such as steam turbine generators sets, compressors, pumps, gas turbine jet engines, turbochargers and electric motors.

In several decades, FEM has been successfully used in rotor dynamic analysis. Gash [1], Nelson and McVaugh [2], Hashish and Sankar [3] used FEM model axi-symmetric rotor bearing system. Jie and Lee [4] model asymmetric rotor bearing system. Ruhl and Booker [5] used FEM analysis rotor only consider translational inertial and bending stiffness. Michael et al. [6],

Giancarlo [7], Thanh et al. [8] proposed a model which included the effects of bending, rotary inertia, gyroscopic moments, transverse shear deformations and axial load in both axi -symmetric and asymmetric rotor bearing system.

In turbo and rotating machines, bearing constitute one of the most critical components. It directly influence on the rotordynamics performance, life, and reliability of the machine. Even after the machine is designed and placed in operation, changes or modifications to the bearings constitute one of the most effective, direct, and economical means to alter and improve the machine's dynamic performance [9]. Bearing-support stiffness depend not only the design and manufacture a particular machines, it also can depend strongly on the way in which that machine is mounted. Natural frequencies and modes are inherent properties of a structure they don't depend on the force or loads acting on the structure. It will change if the characteristic (mass, stiffness, damping) or boundary condition (mounting) of the structure changes [10].

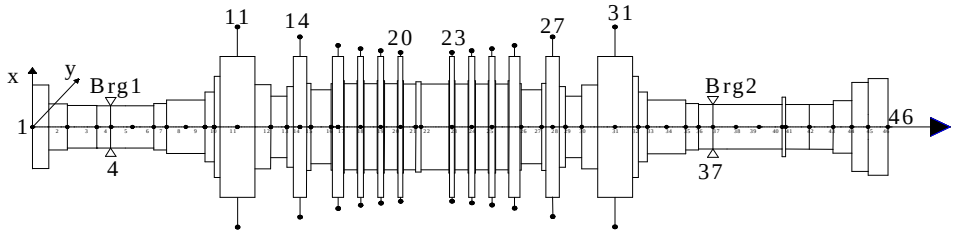

Figure 1. Modeling of a LP B rotor-bearing system.

In this work, the LP B rotor of a 1000 MW USC (ultra-supercritical) steam turbine is studied. Turbo-generator sets with 1000 MW are widely used in generation of electric power. It is a large and complex rotating machine. Figure 1 shows the structure of the LP B rotor-bearing system. The system is modeled 45 Timoshenko beams with 46 nodes, 184 degrees of freedom, including gyroscopic, shear modulus, and rotary inertia effects. Bearings locate at node 4 and node 37 and denote by Brg1 and Brg2. Both bearings have stiffness $k_{xx} = k_{yy} = 2.45\times10^9$ N/m and damping $c_{xx} = c_{yy} = 3\times10^3$ N.s/m.

2. FINITE ELEMENT MODELING ROTOR

A typical shaft element and its coordinate are illustrated in Figure 2. Here, we consider only lateral or transverse vibration so each node has four generalize coordinates: transverse displacements *u*, *v* in the *x*-, *y*- direction and rotation, ψ,θ about *x*- and *y*-axes. A vector $\{q\}^T = \left\{q_1^e ... q_8^e\right\}^T = \{u_{e1}, v_{e1}, \theta_{e1}, \psi_{e1}, u_{e2}, v_{e2}, \theta_{e2}, \psi_{e2}\}^T$ contains the coordinate of an element.

2.1. Shaft elements

The element matrices are derived using energy methods. Because of the symmetric, the mass matrix and the stiffness matrix in the *xz* plane and the *yz* plane are obtained in similar way. The deflection within the element in the *xz* plane (Figure 3) is approximated by [6]

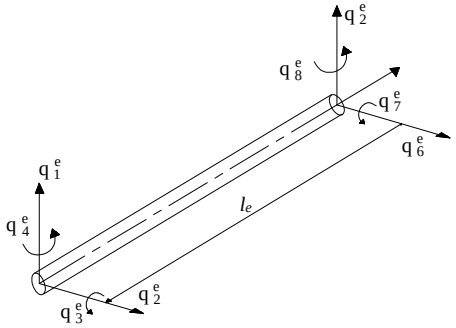

Figure 2. Coordinate used in analysis of rotor.

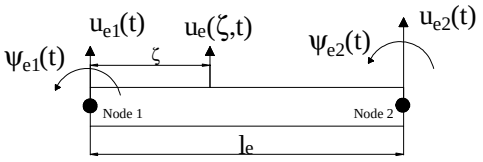

Figure 3. Coordinate in xz plane.

$$u_e(\xi,t)=[N_{e1}(\xi)\ \ N_{e2}(\xi)\ \ N_{e3}(\xi)\ \ N_{e4}(\xi)]\begin{Bmatrix} u_{e1}(t) \\ \psi_{e1}(t) \\ u_{e2}(t) \\ \psi_{e2}(t) \end{Bmatrix} \tag{1}$$

where the shape functions, $N_{ei}(\xi)$, are

$$N_{e1}(\xi)=(1-3\frac{\xi^2}{l_e^2}+2\frac{\xi^3}{l_e^3}) \qquad N_{e2}(\xi)=l_e(\frac{\xi}{l_e}-2\frac{\xi^2}{l_e^2}+\frac{\xi^3}{l_e^3})$$

$$N_{e3}(\xi)=(3\frac{\xi^2}{l_e^2}-2\frac{\xi^3}{l_e^3}) \qquad N_{e4}(\xi)=l_e(-\frac{\xi^2}{l_e^2}+\frac{\xi^3}{l_e^3})$$

Now assume that the cross section do not vary within the element. The strain energy within the beam element is

$$U_e=\frac{1}{2}\int_0^{l_e}E_eI_e(\xi)(\frac{\partial^2u_e(\xi,t)}{\partial\xi^2})^2d\xi=\frac{1}{2}E_eI_e\int_0^{l_e}(\frac{\partial^2u_e(\xi,t)}{\partial\xi^2})^2d\xi \tag{2}$$

where E_e, I_e are the Young's modulus and the second moment of cross-section about the neutral plane respectively. Making the substitution from Eqs. (1) and (2), the strain energy is given by

$$U_e=\frac{1}{2}\{q_e\}^T[K_e]\{q_e\} \tag{3}$$

K_e is element stiffness matrix, given by

$$K_e = \frac{E_e I_e}{l_e^3}\begin{bmatrix} 12 & 6l_e & -12 & 6l_e \\ & 4l_e^2 & -6l_e & 2l_e^2 \\ & symm & 12 & -6l_e \\ & & & 4l_e^2 \end{bmatrix} \tag{4}$$

The mass matrix is computed in a similar way but using the kinetic energy. Neglecting the rotational effect, the kinetic energy of the beam is

$$T_e = \frac{1}{2}\int_0^{l_e} \rho_e A_e \dot{u}_e^2(\xi,t)d\xi = \frac{1}{2}\{\dot{q}_e\}^T[M_e]\{\dot{q}_e\} \tag{5}$$

ρ_e, A_e are the density of the material and cross-section area of the beam respectively. M_e in Eq. (5) is element mass matrix and gives as below

$$M_e = \frac{\rho_e A_e l_e}{420}\begin{bmatrix} 156 & 22l_e & 54 & -13l_e \\ & 4l_e^2 & 13l_e & -3l_e^2 \\ & Symm & 156 & -22l_e \\ & & & 4l_e^2 \end{bmatrix} \tag{6}$$

Based on the local coordinate vector for each element bending in the two planes, the localcoordinate vector is

$$q = \{u_{e1}, v_{e1}, \theta_{e1}, \psi_{e1}, u_{e2}, v_{e2}, \theta_{e2}, \psi_{e2}\}^T .$$

Assuming two bending planes do not couple, the element matrix for the two planes are merely inserted correct location in the 8×8 shaft element matrices.

2.2. Disk elements

The disk elements are assumed to be rigid as four degrees of freedom. The kinetic energy of a disk is [6]

$$T_d = \frac{1}{2}m_d\left(\dot{u}^2 + \dot{v}^2\right) + \frac{1}{2}I_d\left(\omega_{\tilde{x}}^2 + \omega_{\tilde{y}}^2\right) + \frac{1}{2}I_p\omega_{\tilde{z}}^2 \tag{7}$$

where m_d is the mass of the disk, $\dot{u}, \dot{v}$ are the velocities in the x and y directions, I_p, I_d are the polar moment and diametral moment of inertial, $\omega_{\tilde{x}}, \omega_{\tilde{y}}, \omega_{\tilde{z}}$ are the instantaneous angular velocities about $\tilde{x}-, \tilde{y}-, \tilde{z}-$ axes, which are fixed in the disk and rotate with it.

In Eq. (7), the first term is the kinetic energy due to the translation of the disk. The second and the third term are kinetic energy due to the rotational motion of the disk. The detail definition of the $\omega_{\tilde{x}}, \omega_{\tilde{y}}, \omega_{\tilde{z}}$ [6] is

$$\begin{Bmatrix} \omega_{\tilde{x}} \\ \omega_{\tilde{y}} \\ \omega_{\tilde{z}} \end{Bmatrix} = \begin{Bmatrix} \dot{\theta}\cos\phi + \dot{\psi}\sin\phi\cos\theta \\ -\dot{\theta}\sin\phi + \dot{\psi}\cos\phi\sin\theta \\ \Omega - \dot{\psi}\sin\theta \end{Bmatrix} \tag{8}$$

in here, $\dot{\theta}, \dot{\psi}$ are angular velocities about the *x*-, *y*- axes respectively, ϕ is the angular of rotation about the shaft. Assuming the rotations θ and ψ are small, we can neglect terms higher than second order and their derivatives. Take Eq. (8) into Eq. (7) into to obtain

$$T_d = \frac{1}{2} m_d \left(\dot{u}^2 + \dot{v}^2 \right) + \frac{1}{2} I_d \left(\dot{\theta}^2 + \dot{\psi}^2 \right) + \frac{1}{2} I_p \left(\Omega^2 - 2\Omega \dot{\psi}\theta \right) \tag{9}$$

The element matrices are obtained by applying Lagrange's equation to Eq. (9). Thus we have the mass matrix M_e and the gyroscopic matrix G_e of the disk as

$$M_e = \begin{bmatrix} m_d & 0 & 0 & 0 \\ 0 & m_d & 0 & 0 \\ 0 & 0 & I_d & 0 \\ 0 & 0 & 0 & I_d \end{bmatrix} \qquad G_e = \begin{bmatrix} 0 & 0 & 0 & 0 \\ 0 & 0 & 0 & 0 \\ 0 & 0 & 0 & I_p \\ 0 & 0 & -I_p & 0 \end{bmatrix} \tag{10}$$

2.3. Bearings

In general, bearing force on the rotor are normally modeled by stiffness and damping matrices as shown in the following the equation [6-8].

$$\begin{Bmatrix} f_x \\ f_y \end{Bmatrix} = -\begin{bmatrix} k_{xx} & k_{xy} \\ k_{yx} & k_{yy} \end{bmatrix} \begin{Bmatrix} u \\ v \end{Bmatrix} - \begin{bmatrix} c_{xx} & c_{xy} \\ c_{yx} & c_{yy} \end{bmatrix} \begin{Bmatrix} \dot{u} \\ \dot{v} \end{Bmatrix} \tag{11}$$

where, f_x, f_y are the dynamic force in the *x* and *y* direction, *u*, *v* are the dynamic displacements of the shaft journal relative to the bearing housing in the x and y directions. Figure 4 illustrates the stiffness and damping of the journal bearing model. In this paper, k_{xy}, k_{yx}, c_{xy}, c_{yx} are assumed equal zero.

3. EQUATION OF MOTION

Generally, the equation of motion for vibration of a multiple degree of freedom (dof) rotor

– bearing system may be written as

$$M\ddot{q}+(\Omega G+C)\dot{q}+Kq=F(t), \tag{12}$$

where: q is a vector containing the generalized coordinate; M is mass matrix; G is gyroscopic matrix; C is damping matrix; K is stiffness matrix; Ω is rotor spin speed; $F(t)$ is generalized force.

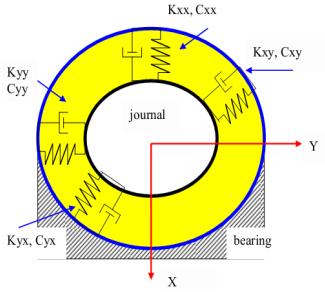

Figure 4. Journal Bearing model

3.1. Free vibration

Free vibration is fundamental to the dynamical of characteristic of rotor system. For free vibration ($F(t) = 0$) and the Eq. (12) rewrite in state-space form [6,7]

$$\begin{bmatrix} C+\Omega G & M \\ M & 0 \end{bmatrix}\frac{d}{dt}\begin{Bmatrix} q \\ \dot{q} \end{Bmatrix}+\begin{bmatrix} K & 0 \\ 0 & -M \end{bmatrix}\begin{Bmatrix} q \\ \dot{q} \end{Bmatrix}=\begin{Bmatrix} 0 \\ 0 \end{Bmatrix} \tag{13}$$

Solving Eq (13) in state space form give the eigenvalues s, it occur as a complex conjugate pairs

$$s_{i,}s_{n+i}=\omega_{ni}\left(-\zeta_i \pm j\sqrt{1-\zeta_i^2}\right)=-\zeta_i\omega_{ni}\pm j\omega_{di} \tag{14}$$

where $\omega_{ni,}\omega_{di,}\zeta_i$ are the natural frequencies, damped natural frequencies and damping ratio respectively, for the i^{th} mode, and $j=\sqrt{-1}$.

3.2. Unbalance response

The vector of generalize force acting at node k due to a disk offset by a displacement ε and an angle β usually represent in form [6], ($\Re$ denotes the real part of the complex number).

$$F_e(t)=\Re\left(\Omega^2\begin{Bmatrix} m_k\varepsilon e^{j\delta} \\ -m_k e^{j\delta} \\ j\left(I_{dk}-I_{pk}\right)\beta e^{j\gamma} \\ \left(I_{dk}-I_{pk}\right)\beta e^{j\gamma} \end{Bmatrix}e^{j\Omega t}\right)=\Re(\Omega^2 b_{0e}e^{j\Omega t}) \tag{15}$$

where δ and γ are the angle (when t = 0) of the out-of–balance force and moment vectors relative to Oxy axes, m_k, $I_{pk,}$ I_{dk}, are the mass, polar moment and diametral moment of inertia of the disk at node k. Taking Eq. (15) into Eq. (12), gives

$$M\ddot{q} + \Omega G\dot{q} + C\dot{q} + Kq = \Re(\Omega^2 b_0 e^{j\Omega t}) \quad (16)$$

Solving Eq. (16) determine the steady-state response to the unbalance forces. Letting $q(t) = \Re(q_0 e^{j\Omega t})$ (q_0 is complex) gives the unbalance response as

$$q_0 = [\left(K - \Omega^2 M\right) + j\Omega(\Omega G + C)]^{-1} \Omega^2 b_0 \quad (17)$$

3.3. Critical Speed

Campbell diagram: The Campbell diagram is the most general method to determine critical speeds. Suppose that for any one frequency component of forcing, the frequency ω_f, can be written in terms of rotational speed

$$\omega_n = f(\Omega) \quad (18)$$

A force whose frequency is identical to rotor speed is said to be a *synchronous force* (n = 1).The critical speeds of the system is given by the intersections of the synchronous line $\omega_f = \Omega$ (ω_f is forcing frequency) and natural frequency curves $\omega_n = f(\Omega)$ [6, 7].

4. CALCULATION RESULTS

4.1. Vibration frequency of the rotor

The first eight eigenvalues, natural frequencies ω_n, for the rotor at 0 rev/min and 3000 rev/min are given in table 1. At zero speed, the natural frequencies occur in pair because in the x- and y- direction, the rotor- bearing system is uncoupled and the inertia and stiffness of the rotor identical. When the shaft is spinning at 3000 rev/min, each pairs of natural frequencies separates due to gyroscopic effect. Because both the shaft and disk of the rotor have large diameters, the influence of gyroscopic is large. The separation of natural frequencies is more clearly illustrated by the Campbell diagram shown in Figure 5. As the shaft speed increase, each natural frequency diverges, one frequency increase and one decrease. The real part of roots is very small, damping ratio approximately equals zero so that damped natural frequencies are very close to natural frequencies.

4.2. Unbalance response

It's assumed that an out-of-balance of 0.001 m acts on the two sides of the rotor (disk 11 and disk 31) in the same angular position (Figure 1). Unbalance responses of the rotor are analyzed in two cases: (1) the rotor supported by isotropic bearings and (2) anisotropic bearings.

Table 1. The first eight eigenvalues and natural frequencies.

0 rev/min		3000 rev/min	
Root s (rad/s)	ω_n (Hz)	Root s (rad/s)	ω_n (Hz)
$-3.92\times10^{-3}\pm 141.50j$	22.52	$-3.6\times 10^{-3}\pm 139.47j$	22.19
$-3.92\times10^{-3}\pm 141.50j$	22.52	$-4.24\times10^{-3}\pm143.46j$	22.83
$-2.06\times10^{-2}\pm 281.95j$	44.87	$-1.96\times10^{-2}\pm 144.86j$	43.63
$-2.06\times10^{-2}\pm 281.95j$	44.87	$-2.15\times10^{-3}\pm 289.82j$	46.12
$-4.86\times10^{-2}\pm 368.67j$	58.67	$-4.55\times10^{-2}\pm 354.96j$	56.50
$-4.86\times10^{-2}\pm 368.67j$	58.67	$-5.16\times10^{-2}\pm382.31j$	60.85
$-2.43\times10^{-2}\pm 454.47j$	72.31	$-2.46\times10^{-2}\pm 436.27j$	69.44
$-2.43\times10^{-2}\pm 454.47j$	72.31	$-2.38.\times0^{-2}\pm 473.10j$	75.23

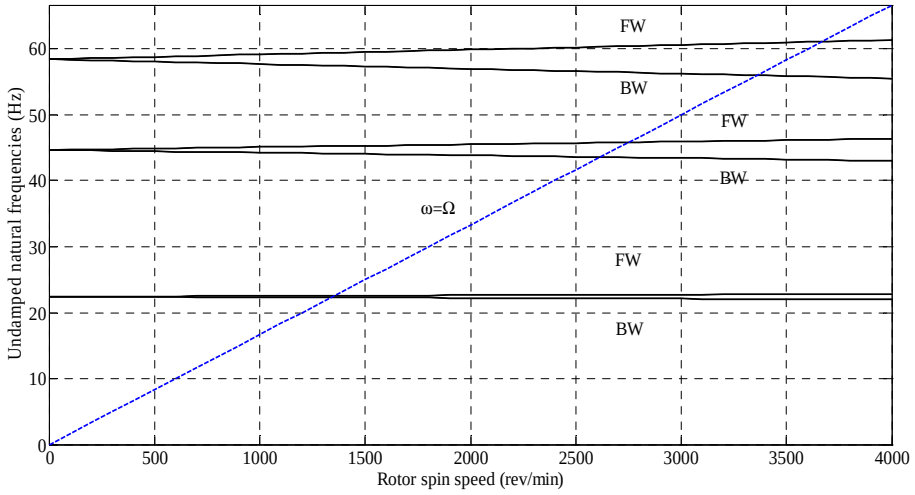

Figure 5. Campbell diagram, FW (forward whirl), BW (backward whirl).

4.2.1. Rotor Supported by Isotropic bearings

In this case, the bearings stiffness matrices are symmetric with the original stiffness $k_{xx}= k_{yy} = 2.45 \times 10^9$ N/m and damping $c_{xx} = c_{yy} = 3\times10^3$ N.s/m.

Figure 6 shows unbalance responses and phase changes of these nodes to *x* direction. Because of the symmetric system, the responses in the *x* direction and in the *y* direction are coincided. The responses to the out-of-balance force at the equivalent critical speeds of 1360,

2750, and 3680 rev/min get maximum values. Comparing with the rotor speeds, these speeds coincide with natural frequencies of the system in the Campbell diagram (figure 5) and only forward whirl modes are exited. When the rotor spins at sub-critical speed range, these nodes whirl in-phase. Due to critical speeds, the phases change by approximately 180^o (because of damping, the phase change do not exactly by 180^o). The phase changes occur at both resonances and anti resonances of the system. The phase of the node 11 reverses two times in regions 2250 rev/min and 2890 rev/min, respectively. The node 31 also reverse phase in region 3050 rev/min.

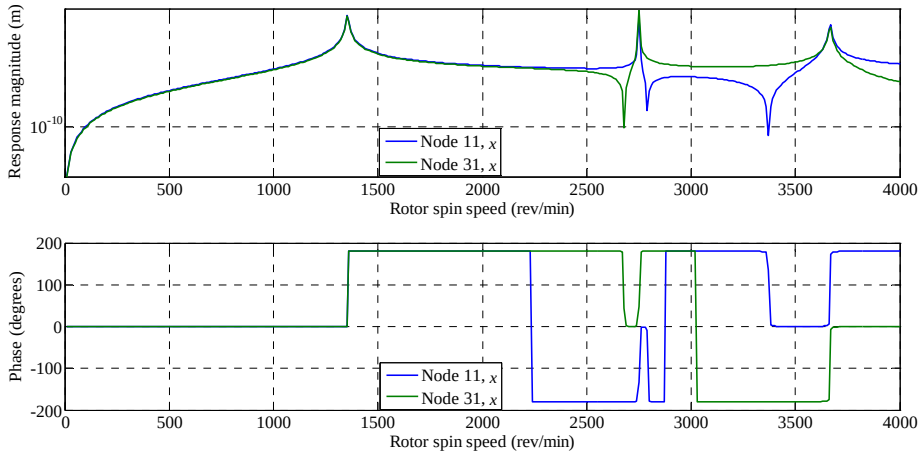

Figure 6. Unbalance response of the rotor at node 11, 31 in the × direction.

4.2.2. Rotor Supported by anisotropic bearing

This system is the same with previous system, except that the isotropic bearings are replaced by anisotropic bearings. Original stiffness of each bearing is assumed to be $k_{xx} = 2.45 \times 10^9$ N/m and will be changed, by $k_{yy} = 2.40 \times 10^9$ N/m.

The responses of the system at node 11 and node 31 to out-of-balance 0.001m on both disks (at node 11 and node 31) are shown in Figure 7. The responses have a maximum when rotor speeds is 1340, 1360, 2620, 2760, 3360 and 3670 rev/min. Comparing these speed with the critical speed of the rotor in the Campbell diagram, we can see that both forward and backward modes are excited. The stiffness of the system is difference in *x* and *y* directions; hence, the amplitude of whirl in these directions are difference, this illustrated in Figure 8.

It can be seen that, the peaks response occur at the same rotor speed in the *x* and *y* directions. At these speeds, responses of phases are changed. The zero values of the response in *x* and *y* direction occur at different rotor speeds; thus the phase of response in the *x* direction changes at a different rotor speed from that the *y* direction. If the phase of response in either *x* or *y* direction changes substantially, the direction of whirl reverse. In Figure 8, regions of backward whirl are indicated by shaded regions. At some rotor speeds, one part of the rotor is in backward

whirl whereas other is in forward whirl (mix mode). It is more clearly by plot orbits at these nodes as shown in Figure 9. The orbits are elliptical and can be forward or backward.

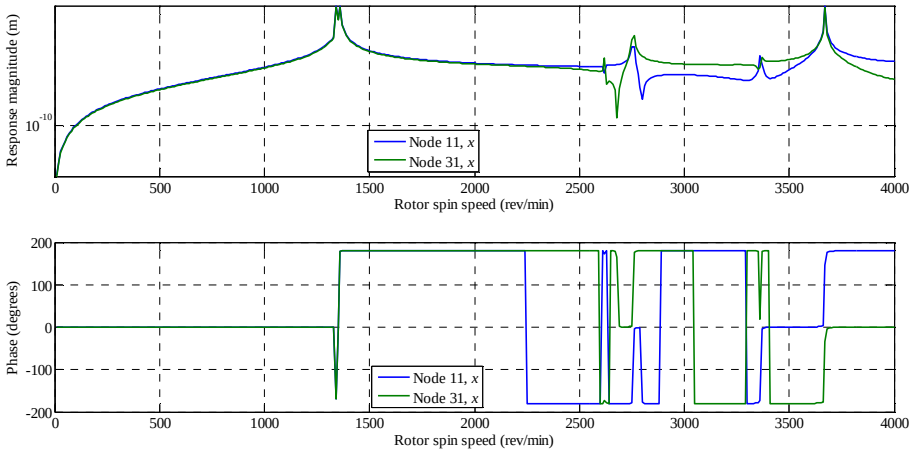

Figure 7. Response of the rotor at node 11 and node 31 in x direction due to out-of-balance force at node 11 and node 31 (the length of the semimajor axis of the orbit).

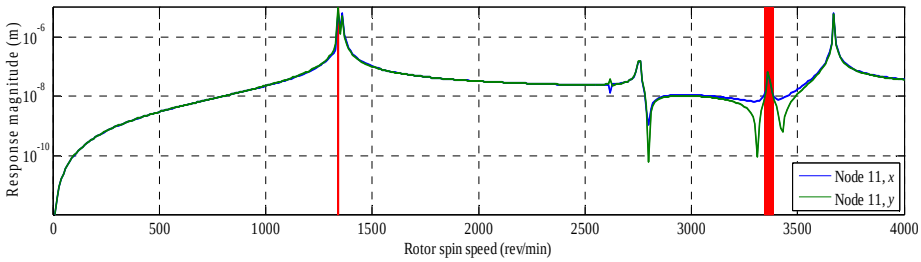

Fi.ureg 8. Response in x and y direction at node 11, the red shaded region indicates backward whirl.

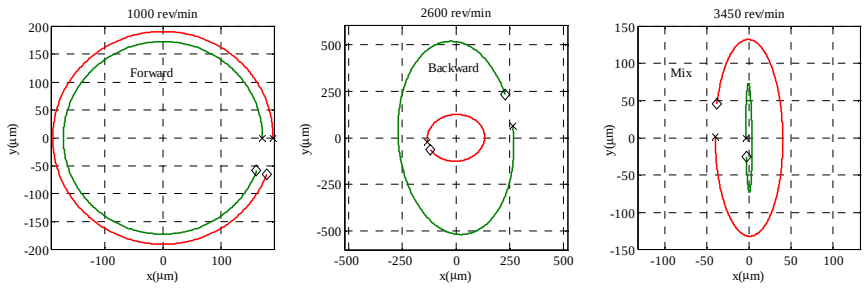

Figure 9. Whirl orbits at node 11 (dashed) and node 31 (solid) for the rotor on anisotropic bearings. The cross denotes the start of the orbit and the diamond denotes the end

4.2.3. Map of critical speed and mode shapes

Map of critical speed and mode shapes enable an engineer to obtain rapidly an impression of how the uncertainly in one of the parameters affect behavior of the machine. Figure 10 shows how the first two mode shapes of the rotor vary with the bearing stiffness. It can be seen that, at low stiffness ($10^8 \div 10^9$ N/m), the rotor is hardly constrained and the mode shape are more various. At high stiffness, the bearing presents an almost pinned constraint and the mode shapes of the rotor do not change. That means, the bearing can be considered as a rigid body approximately.

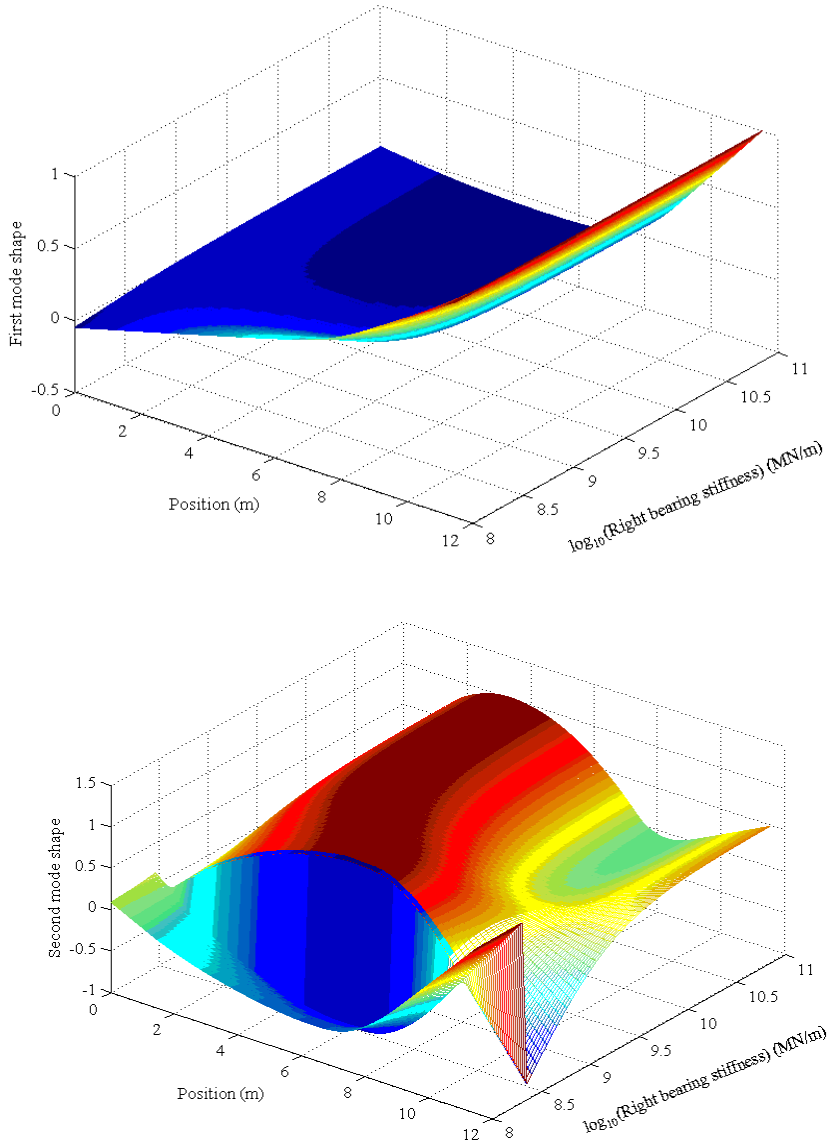

Figure 10. The variation of the first two mode shape with bearing stiffness.

5. CONCLUSTIONS

In this study, the dynamic vibration behavior of the LB B rotor of a 1000 MW turbo-generator under unbalance forces is investigated. The finite element method (FEM) is applied to model the system. The results can be summarized as follows:

The responses of the rotor in two case isotropic and anisotropic bearing systems are analyzed. In case the rotor supported by isotropic bearing, only forward modes are excited. Whereas in case of the rotor supported by anisotropic bearings, both forward and backward modes are excited

The influence of the bearing support stiffness on critical speed and mode shape is one of the most basic principles. This map is generated through a parametric variation of the bearing support stiffness. It provides an overview of how the critical speeds and mode shapes will change with variation of the bearing support stiffness.

REFERENCES

1. Gash R. - Vibration of Large Turbo-Rotor in Fluid-Film bearing on Elastic Foundation, Journal of Sound and Vibration **47** (1) (1976) 53 -73.
2. Nelson H. D., McVaugh J. M. - The dynamic of rotor-bearing systems using finite elements, Journal of Engineering for Industry **98** (2) (1976) 593–599.
3. Hashish E., Sankar T. S. - Finite Element and Modal Analysis of Rotor-bearing system Under Stochastic Loading Condition, Journal of Vibration and Acoustics **106** (1) (1984) 80-89.
4. Jie Y., Lee C. - Finite Element Modal of Asymmetrical Rotor-Bearing systems, KSME Journal **2** (2) (1988) 116–124.
5. Ruhl R, Booker J. F. - A Finite Element Model for Distribute Parameter Turbo Rotor System, ASME journal of Engineering for Industry **94** (1972) 126–132.
6. Friswell M. I., Penny J. E. T., Garvey S. D., Lees A. W. - Dynamics of Rotating Machines, Cambridge University Press, 2010, pp 155-200.
7. Genta G. - Dynamics of rotating systems, Springer, 2005, pp. 282-291.
8. Ngo V. T., Xie D. M., Zhang H. L., Xiong Y. H., Yang Y. - Dynamic analysis of a rig shafting vibration based on finite element, Front. Mech. Eng. **8** (3) (2013) 244-251.
9. Vance J., Zeidan F., Murphy B. - Machinery vibration and Rotordynamics. John wiley & Songs, 2010, pp 171-190.
10. Luo J., Liu Z., Shi Y., Xie D., Yu X. - The Research on Supporting Stiffness of LP Rotor of Ultra-supercritical Turbine, 2011 ICECE-LJB (IEEE) (2011) 1846-1848.

TÓM TẮT

PHÂN TÍCH MÔ HÌNH DAO ĐỘNG CỦA TURBINE BẰNG PHƯƠNG PHÁP PHẦN TỬ HỮU HẠN

Ngô Văn Thanh[1,*], Danmei Xie[2], Lê Hoài Đức[1]

[1]*Trường Đại học Giao thông vận tải, Việt Nam*

[2]*Viện Cơ khí động lực, Đại học Vũ Hán, Trung Quốc*

[*]Email: *ngovanthanhdc@gmail.com*

Phương pháp phần tử hữu hạn được ứng dụng rộng rãi trong tính toán sức bền, dao động, nhiệt động cũng như rất nhiều lĩnh vực khác trong tính toán thiết kế cơ khí. Trong những năm gần đây, với việc phát triển mạnh mẽ của máy tính, phương pháp phần tử hữu hạn đã được sử dụng chủ yếu để tính toán tĩnh và động lực học của hệ rotor và ổ trục. Bài báo nghiên cứu dao động ngang của turbine máy phát điện cỡ lớn bằng phương pháp phần tử hữu hạn. Từ mô hình phần tử hữu hạn, tác giả tiến hành phân tích các đặc trưng của hệ dao động bao gồm tần số dao động tự do, tốc độ tới hạn, trạng thái dao động riêng. Trạng thái mất cân bằng được phân tích và so sánh khi turbine lắp trên ổ trục đẳng hướng và ổ trục bất đẳng hướng.

Từ khóa: phương pháp phần tử hữu hạn (FEM), dao động ngang, turbine, trạng thái dao động, tốc độ tới hạn.